Available online at www.sciencedirect.com
ScienceDirect
Ceramics International 35 (2009) 3537–3540
CERAMICS INTERNATIONAL
www.elsevier.com/locate/ceramint

Short communication

($h\ k\ i\ l$)-specific G.P. zones in Sn- versus Zr-doped α-Al_2O_3 by solution annealing

Jer-Han Lu, I.-Lung Liu, Pouyan Shen *

Department of Materials and Optoelectronic Science, National Sun Yat-sen University, Kaohsiung, Taiwan, ROC

Received 13 May 2009; received in revised form 19 May 2009; accepted 5 June 2009
Available online 7 July 2009

Abstract

The α-Al_2O_3 powder doped with Sn or Zr via a solid-state sintering route was annealed for a comparative study of Guinier-Preston (G.P.) zone by electron microscopy. The 2 at.% Sn-doped α-Al_2O_3 showed G.P. zones plates with coherent habit planes parallel to (0 0 0 1) and ($\bar{1}$ 2 $\bar{1}$ 0). The 0.6 at.% Zr-doped α-Al_2O_3 showed similar shaped G.P. zones but with more corrugated (0 0 0 1) plane. The habit plane selection can be rationalized by anisotropic solute expulsion along relatively close packed (0 0 0 1) and ($\bar{1}$ 2 $\bar{1}$ 0) planes under the influence of a precondensation effect analogous to that reported for a crystallization process. Solute-specific volume and charge-compensating defects account for the coherency strain difference of the G.P. zones in α-Al_2O_3.

Keywords: A. Firing; B. Defects; B. Impurities; D. Al_2O_3

1. Introduction

The effect of rather limited solid solution and exsolution of the aliovalent cation Sn^{4+} versus Zr^{4+} on the formation of metastable precipitates and planar defects in Al_2O_3 lattice has been investigated.

The rock-salt type metal monoxide doped with aliovalent cation, such as Zr-doped $Ni_{1-x}O$ [1], showed paracrystalline distribution of defect clusters when solution annealed. The TiO_2 rutile doped with Zr^{4+} [2] or Zn^{2+} [3], however, showed (1 0 0) and (0 1 0)-specific Guinier-Preston (G.P.) zone plates besides other planar defects and commensurate superstructures when solution annealed. In the case of Zr^{4+}-doped TiO_2, incommensurate as well as commensurate superstructures with triple (1 0 1) and (1 1 1) periodicity also occurred as metastable intermediates [2]. As for the case of Zn^{2+}-doped TiO_2, a rather limited solid solution and exsolution of the aliovalent cation Zn^{2+} typically caused the formation of crystallographic shear (CS) [3]. The resultant CS slip planes turned out to be similar to those of undoped Ti_nO_{2n-1}, thus shedding light on the concentration of charge-compensating oxygen vacancies in Zn^{2+}-doped TiO_2 [3].

Here we report ($h\ k\ i\ l$)-specific G.P. zones in Zr^{4+}- versus Sn^{4+}-doped α-Al_2O_3 with a corundum-type structure (space group $R\bar{3}c$) and a rather limited solid solubility [4,5].

2. Experimental

The Al_2O_3 powder (Cerac 99.9% <147 μm in diameter, denoted as A) mixed with SnO_2 (Alfa Aesar, 99.9%, <10 μm, denoted as S) or ZrO_2 (Aldrich 99.95%, <3 μm, denoted as Z) in a fixed mole ratio of 8:92, denoted as A8S92 and A8Z92, respectively, were dry-pressed at 650 MPa to form pellets 10 mm in diameter and 2 mm in thickness. The A8S92 pellets were sintered at 1500 °C for 24 h followed by air quenching and then annealing at 1000 or 1100 °C for up to 140 h in air. The relatively inert A8Z92 pellets were sintered at a higher temperature (1600 °C) for 24 h and then annealed at 1200 °C for up to 72 h in air. After firing, the minor Al_2O_3 component in the fired A8S92 and A8Z92 specimens occurred as inter- and intra-granular particles in a host of SnO_2 and ZrO_2 of rutile- and fluorite-type derived structures, respectively. The Al_2O_3-rich compositions A92S8 and A92Z8 turned out to have inter- and intra-granular particles of SnO_2 and ZrO_2, respectively in a host of Al_2O_3 grains which showed the same ($h\ k\ i\ l$)-specific G.P. zones when solution annealed under the

* Corresponding author. Tel.: +886 7 5254060; fax: +886 7 5254099.
E-mail address: pshen@mail.nsysu.edu.tw (P. Shen).

0272-8842/$36.00
doi:10.1016/j.ceramint.2009.06.001

same conditions as for the Al_2O_3-poor samples [6,7]. In other words, the metastable precipitate and defect formation of the Sn- and Zr-doped α-Al_2O_3 upon solution annealing is not affected by it being a major or minor phase in the sintered composite.

The d-spacings measured from X-ray diffraction (XRD, Cu Kα, 40 kV, 30 mA, Siemens D5000) traces [6,7] were used for least-squares refinement of the lattice parameters of the predominant α-Al_2O_3 doped with Sn or Zr in the A92S8 and A92Z8 specimens [6,7]. Thin sections of the fired samples were Ar-ion milled to electron transparency for transmission electron microscopic (TEM, JEOL3010, 300 kV) observations coupled with energy dispersive X-ray (EDX) analysis.

3. Results

XRD and scanning electron microscopic observations [6,7] indicated that the as-sintered A8S92 and A8Z92 samples have intra- and inter-granular α-Al_2O_3 particles which were confined in the host SnO_2 and ZrO_2 grains of rutile- and fluorite-type derived structures, respectively.

TEM observations indicated that the Sn-doped Al_2O_3 particles, either as-sintered [6] or further annealed, contain disk-like G.P. zones with diffraction and strain contrast. Such G.P. zones have habit planes parallel to (0 0 0 1) and $(\bar{1}\,2\,\bar{1}\,0)$ as indicated by bright field image (BFI) and corresponding selected area electron diffraction (SAED) pattern of a representative particle in $(1\,0\,\bar{1}\,0)$ zone axis (Fig. 1a and b) and another particle in $(\bar{1}\,2\,\bar{1}\,0)$ zone axis (Fig. 1c and d). Lattice image (Fig. 1e) and 2-D Fourier transform (Fig. 1f) further indicated that the lattice planes $(1\,0\,\bar{1}\,\bar{2})$, $(1\,0\,\bar{1}\,4)$ and (0 0 0 6) are coherent with respect to the (0 0 0 1) habit plane when viewed edge on. (The disk-like G.P. zones are also coherent with respect to the lattice planes $(\bar{1}\,2\,\bar{1}\,0)$, $(0\,1\,\bar{1}\,2)$ and $(1\,\bar{1}\,0\,2)$ when viewed in $(2\,0\,\bar{2}\,\bar{1})$ zone axis [6].) Point-count EDX analysis (Fig. 1g) indicated that the Sn-doped α-Al_2O_3 contains ca. 2 at.% Sn regarding the solute expulsion to form the G.P. zones.

TEM observations of the as-sintered A8Z92 specimen indicated that Zr-doped α-Al_2O_3 particle (Fig. 2) also contains disk-like G.P. zones with diffraction and strain contrast. The BFI and SAED pattern (Figs. 2a and b, respectively) of such a particle in $(2\,\bar{2}\,0\,1)$ zone axis indicated that the G.P. zones have a specific habit plane parallel to $(1\,1\,\bar{2}\,0)$ edge on. This accounts for the slight streaking of the diffraction spots along the $(1\,1\,\bar{2}\,0)$ plane normal. Lattice image (Fig. 2c) and 2-D Fourier transform (Fig. 2d) further showed that the $(0\,1\,\bar{1}\,2)$ and $(1\,0\,\bar{1}\,\bar{2})$ planes are slightly distorted across the G.P. zones. Point-count EDX analysis of this particle (Fig. 2e) indicated that the Zr content is ca. 0.6 at.%. The G.P. zones in the annealed A8Z92 samples showed more significant diffraction contrast in the BFI (Fig. 3a) and (0 0 0 1)-specific diffraction streaking in the SAED pattern (Fig. 3b) when viewed in the $(1\,0\,\bar{1}\,0)$ zone axis. Lattice image (Fig. 3c) and 2-D Fourier transform (Fig. 3d) showed the (0 0 0 1) planes are extensively distorted across the G.P. zones in this case.

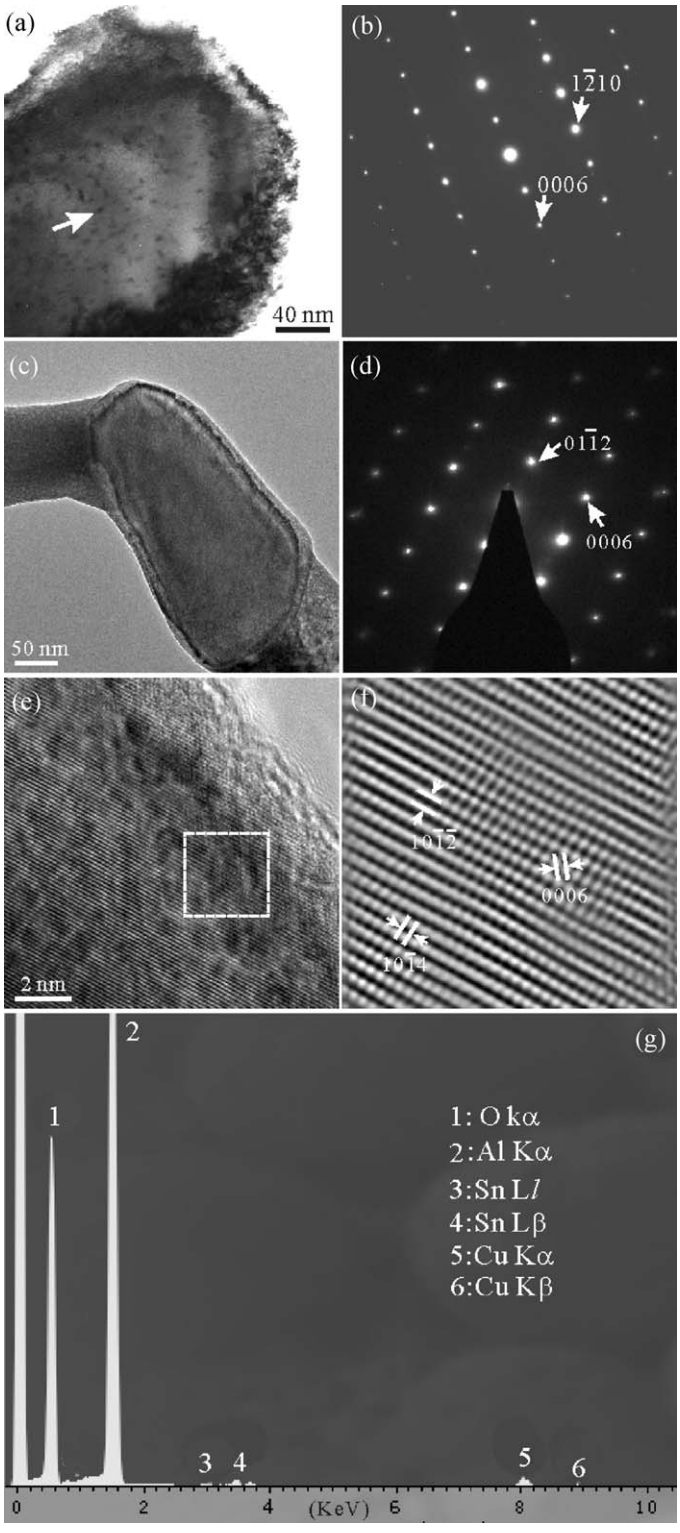

Fig. 1. TEM BFI and corresponding SAED pattern of the G.P. zone plates (arrow) in Sn-doped α-Al_2O_3 particle: (a) and (b) in $(1\,0\,\bar{1}\,0)$ zone axis, (c) and (d) in $(\bar{1}\,2\,\bar{1}\,0)$ zone axis for the A8S92 sample sintered at 1500 °C followed by annealing at 1100 °C and 1000 °C for 72 h, respectively. (g) EDX spectrum of Sn-doped α-Al_2O_3 particle in the A8S92 sample annealed at 1000 °C for 140 h.

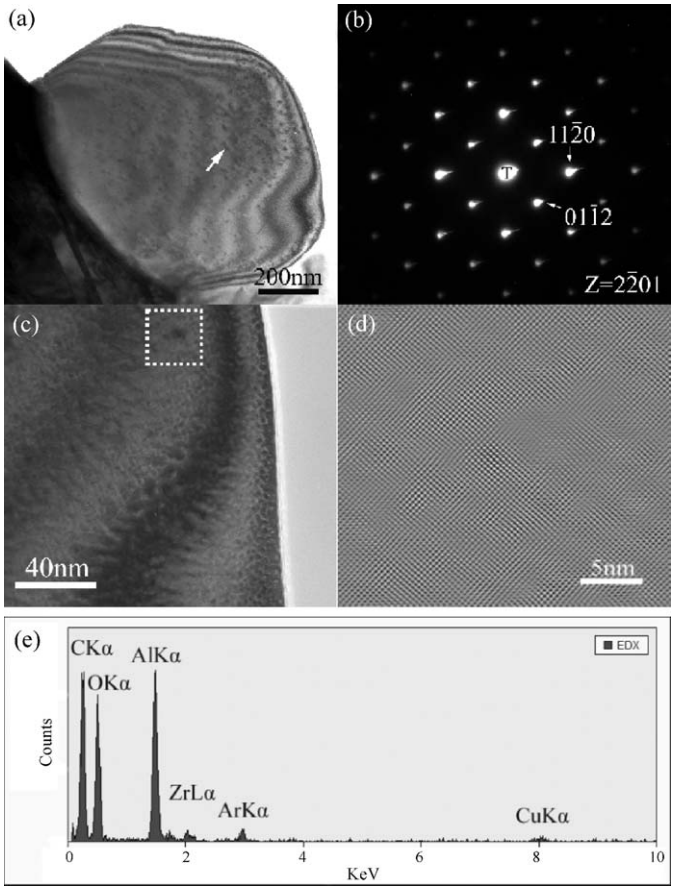

Fig. 2. TEM (a) BFI and (b) SAED pattern of the G.P. zone plates (arrow) in Zr-doped α-Al_2O_3 particle ($Z = (2\,\bar{2}\,0\,1)$) of the A8Z92 sample sintered at 1600 °C for 24 h. (c) Lattice image from local area of (a). (d) 2-D Fourier transform of the square region in (c) showing slightly distorted $(0\,1\,\bar{1}\,2)$ and $(1\,0\,\bar{1}\,\bar{2})$ planes across the G.P. zones. (e) EDX spectrum of Zr-doped α-Al_2O_3 particle in the as-sintered A8Z92 sample.

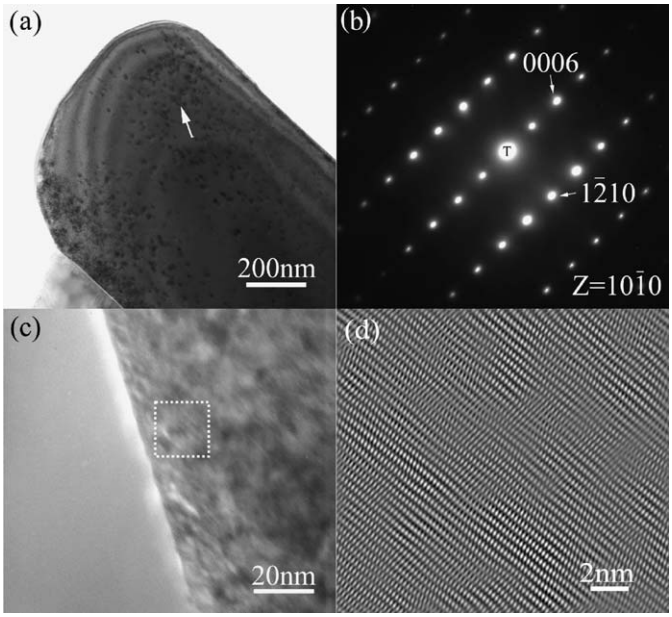

Fig. 3. TEM (a) BFI and (b) SAED pattern of the G.P. zone plates (arrow) in Zr-doped α-Al_2O_3 ($Z = (1\,0\,\bar{1}\,0)$). (c) Lattice image and (d) 2-D Fourier transform of the square region in (c) showing extensively distorted (0 0 0 1) plane across the G.P. zones. A8Z92 sample sintered at 1600 °C for 24 h followed by annealing at 1200 °C for 72 h.

4. Discussion

4.1. Anisotropic growth of G.P. zones

The corundum-type structure has the cation-filled octahedral sites assembled as specific periodic bond chains (PBCs) in terms of strong bonding [8]. The habit plane selection of the G.P. zones in this structure, as characterized by this study, can be rationalized by preferential solute expulsion along the most close packed plane, i.e. (0 0 0 1), rather than $(0\,1\,\bar{1}\,2)$, $(1\,1\,\bar{2}\,0)$ and $(\bar{1}\,1\,0\,4)$, which are F, S and K faces with 2, 1 and 0 PBCs, respectively (cf. [9]). The $(1\,1\,\bar{2}\,0)$ could be relatively favorable than $(0\,1\,\bar{1}\,2)$ under the solute influence, i.e. analogous to the precondensation effect for the unusual surface formation during the crystal growth [10]. Anisotropic expulsion of solute was also observed for the spinodal decomposition in TiO_2–SnO_2 binary [11] although to a much larger extent than the present case of G.P. zone precipitation.

4.2. Defect chemistry due to Sn^{4+} and Zr^{4+} dopant

The Al^{3+}, Sn^{4+} and Zr^{4+} ions have an effective ionic radius of 0.054 nm, 0.069 nm and 0.072 nm, respectively, in coordination number (CN) 6 [12]. Thus, there is a larger misfit of metal ion Zr^{4+} than Sn^{4+} (both denoted as M) in substitution for Al^{3+} in the octahedral sites of the corundum-type structure with charge and volume compensating defects through the following equation in Kröger and Vink notation [13]:

$$3MO_2 \xrightarrow{Al_2O_3} 3M_{Al}^{\bullet} + V_{Al}^{'''} + 6O_o$$

Alternatively, M^{4+} may enter interstitial octahedral sites to form charge and volume compensating Al vacancies via the following equation

$$3MO_2 \xrightarrow{Al_2O_3} 3M_i^{\bullet\bullet\bullet\bullet} + 4V_{Al}^{'''} + 6O_o$$

Such defect reactions agree with a slightly larger XRD cell parameters for Sn-doped ($a = 0.4766 \pm 0.0002$ nm and $c = 1.3018 \pm 0.0008$ nm, [6]) and Zr-doped Al_2O_3 ($a = 0.4759 \pm 0.0001$ nm and $c = 1.3005 \pm 0.0006$ nm, [7]) than the undoped case ($a = 0.4759$ nm and $c = 1.2993$ nm, JCPDS file 46–1212). The Sn-doped Al_2O_3 has a larger unit cell than Zr-doped Al_2O_3 despite a smaller ionic radius of Sn^{4+} than Zr^{4+} in CN 6. This can be explained by a larger solid solubility of Sn^{4+} than Zr^{4+} as mentioned, and the possible presence of Sn^{3+} (0.096 nm in CN 6, [12]) in α-Al_2O_3. Aside from the exact defect clustering scheme to be clarified in future spectroscopic study, the segregation of larger-sized Zr^{4+} than Sn^{4+} to form G.P. zones would cause more significant distortion of the corundum lattice as observed in this study. In the absence of dopant, the Al_2O_3 via a dynamic [14] or static heating process [15] would otherwise be immune from the G.P. zones.

It is worthwhile to note that the coherency of disk-like G.P. zones was not lost upon cooling. This indicates that the

coherency stress was not high enough to cause dislocations despite the elastic [16] and thermal expansion [17] anisotropy of the corundum lattice. The cation vacancies associated with the dopant interstitial, if any, could also help relax the corundum lattice.

5. Conclusions

1. Both Sn- and Zr-doped α-Al_2O_3 formed G.P. zone plates when solution annealed.
2. The habit planes of the G.P. zones can be rationalized by anisotropic solute expulsion along relatively close packed $(0\,0\,0\,1)$ and $(\bar{1}\,2\,\bar{1}\,0)$ planes.
3. The segregation of relatively large-sized Zr^{4+} than Sn^{4+} as G.P. zones caused more significant distortion and corrugation of the corundum-type lattice planes.

Acknowledgements

Supported by Center for Nanoscience and Nanotechnology at NSYSU and National Science Council, Taiwan, ROC.

References

[1] J. Chen, P. Shen, Defect clusters and superstructures of Zr^{4+} dissolved $Ni_{1-x}O$, J. Solid State Chem. 140 (1998) 361–370.
[2] K.C. Yang, P. Shen, D. Gan, Defect microstructures of TiO_2 rutile due to Zr^{4+} dissolution and expulsion, J. Solid State Chem. 179 (2006) 3478–3483.
[3] T. Chen, P. Shen, Defect clustering and ordering in Zn-doped TiO_2 upon solution annealing, J. Phys. Chem. C 113 (2009) 328–332.
[4] V.J. Barczak, R.H. Insley, Phase equilibria in the system Al_2O_3–SnO_2, J. Am. Ceram. Soc. 45 (1962) 144.
[5] E.M. Levin, C.R. Robbins, H.F. McMurdie, Phase diagrams for ceramics, Am. Ceram. Soc. (1969) (Columbus, Ohio).
[6] I.L. Liu, Metastable exsolution in Al_2O_3–SnO_2 binary and early stage sintering of nanosized Al_2O_3, MS Thesis, National Sun Yat-sen University, Taiwan, 2007.
[7] J.H. Lu, Exsolution of ZrO_2-dissolved Al_2O_3 and early stage sintering of nanosized ZrO_2, MS Thesis, National Sun Yat-sen University, Taiwan, 2007.
[8] P. Hartman, W.G. Perdok, On the relations between structure and morphology of crystals. I, Acta Cryst. 8 (1955) 49–52.
[9] C.H. Lin, P. Shen, S.Y. Chen, Y. Zheng, Condensation and crystallization of amorphous/lamellar chromium sesquioxide, J. Phys. Chem. C 112 (2008) 17559–17566.
[10] P. Hartman, W.G. Perdok, On the relations between structure and morphology of crystals. II, Acta Cryst. 8 (1955) 521–524.
[11] H.C. Yu, P. Shen, Phase transformation and microstructures of TiO_2–SnO_2 due to solution annealing vs. reactive sintering, J. Eur. Ceram. Soc. 28 (2008) 91–99.
[12] R.D. Shannon, Revised effective ionic radii and systematic studies of interatomic distances in halides and chalcogenides, Acta Crystallogr. A 32 (1976) 751–767.
[13] F.A. Kröger, H.J. Vink, Relations between the concentrations of imperfections in crystalline solids, Solid State Phys. 3 (1956) 307–435.
[14] C. Pan, S.Y. Chen, P. Shen, Laser ablation condensation, coalescence and phase change of dense γ-Al_2O_3 particles, J. Phy. Chem. B 110 (2006) 24340–24345.
[15] I.L. Liu, P. Shen, Onset coarsening/coalescence kinetics of γ-type related Al_2O_3 nanoparticles: implications to their assembly in a laser ablation process, J. Eur. Ceram. Soc. 29 (2009) 2235–2248.
[16] T. Goto, O.L. Anderson, Elastic constants of corundum up to 1825 K, J. Geophys. Res. 94 (1989) 7588–7602.
[17] H. Zhu, L.A. Tessaroto, R. Sabia, V.A. Greenhut, M. Smith, D.E. Niesz, Chemical mechanical polishing (CMP) anisotropy in sapphire, Appl. Surf. Sci. 236 (2004) 120–130.